JACS Au
AN OPEN ACCESS JOURNAL OF THE AMERICAN CHEMICAL SOCIETY

pubs.acs.org/jacsau
Article

Three Distinct Oxidation States (II/II, II/III, and III/III) of Diorganocopper Complexes

Kai Hua,[§] Fei Xie,[§] Shengfa Ye,* and Ming-Tian Zhang*

Cite This: *JACS Au* 2024, 4, 4406−4414

Read Online

ACCESS | Metrics & More | Article Recommendations | Supporting Information

ABSTRACT: In this report, we present a structurally and spectroscopically characterized diorganocopper system in three distinct oxidation states: [$Cu^{II}Cu^{II}$] (**1**), [$Cu^{II}Cu^{III}$] (**2**), and [$Cu^{III}Cu^{III}$] (**3**). These states are stabilized by a macrocyclic ligand scaffold featuring two square-planar coordination {$C_2^{NHC}N_2^{pyrazole}$}. We have analyzed the geometric and electronic structures using X-ray diffraction (XRD) and multiple spectroscopic methods including nuclear magnetic resonance (NMR), UV−vis, and electron paramagnetic resonance (EPR) spectroscopies, in combination with density functional theory (DFT) calculations. Remarkably, this study provides a structural determination of mixed-valence diorganocopper(II,III) complex **2**, which is at the borderline between valence-trapped or charge-localized class I systems and charge moderately delocalized class II systems in Robin and Day classification. These findings enhance our understanding of the systematic structural and electronic changes that occur in diorganocopper complexes in response to redox transformations.

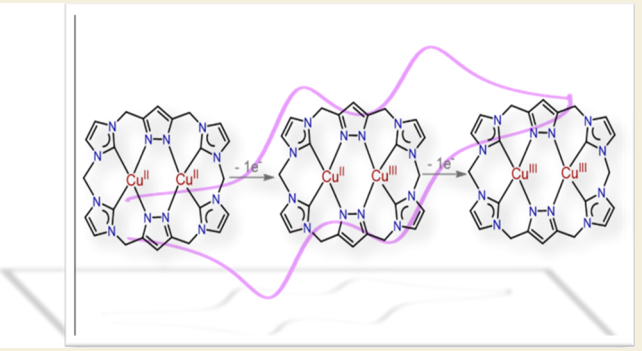

KEYWORDS: *high-valent organocopper complex, macrocycle carbene ligand, oxidation states, structure and electronic state, mixed-valence complex*

INTRODUCTION

The exploration of copper complexes is fundamentally significant due to their remarkable versatility in catalyzing various chemical-bond-forming reactions[1−7] and biological oxidation processes.[8−20] Notably, the copper ion typically exploits changes in its oxidation state to facilitate these copper-mediated reactions.[21−33] Consequently, the synthesis, structure, reaction mechanisms, and synthetic application of organocopper species across various oxidation states have been extensively researched. Prior to the 1990s, high-valent organocopper compounds were considered rare and intrinsically unstable. Since the first structurally well-defined high-valent organocopper(III) species was reported in 2000,[34] the majority of successful examples are supported by macrocyclic chelating ligand, as Cu^{III} ions prefer square-planar coordination (Figure 1a).[5,22,24,28,29,35−45] Despite the significant achievements made in monoorganocopper(III), the stable and well-defined high-valent binuclear copper compounds remain in their infancy, due to a scarcity of ligand scaffolds capable of stabilizing binuclear copper in various states. To date, only two structurally characterized diorganocopper(III,III) compounds have been reported (Figure 1b).[17,46] Besides, the Tolman group reported spectroscopy and theory of hydroxo-bridged mixed-valent $Cu^{II}Cu^{III}$ and symmetric Cu^{III} Cu^{III} species.[11] Therefore, a system that enables the isolation and study of high-valent binuclear copper complexes in the relevant [$Cu^{II}Cu^{II}$], [$Cu^{II}Cu^{III}$], and [$Cu^{III}Cu^{III}$] states presents both attractive and challenging prospects.

Over the past few years, N-heterocyclic carbene ligands (NHCs) have been widely used to trap reactive intermediates in unusual oxidation states, owing to their strong σ-donating properties.[47−51] For instance, recent studies by the Meyer group revealed that the macrocycles {py_2NHC_2} (L′, py = pyridine) and {py_2NHC_4} (L), featuring combinations of pyridine and NHC donors, exhibit great flexibility and support a series of mononuclear Cu complexes in oxidation states of +I, +II, and +III, as well as binuclear complexes $[LCu_2]^{2/3+}$ in the Cu^ICu^I and mixed-valent $Cu^{1.5}Cu^{1.5}$ states, respectively.[37,52] Interestingly, despite large structural changes, mixed-valent $Cu^{1.5}Cu^{1.5}$ complex was fully delocalized and fast electron self-exchange rate. Moreover, the majority of the literature suggests that most reported NHC-Cu^{II} complexes required the addition of chelating N- or O-donors, often contain anionic coligands,

Received: August 15, 2024
Revised: September 26, 2024
Accepted: September 26, 2024
Published: October 16, 2024

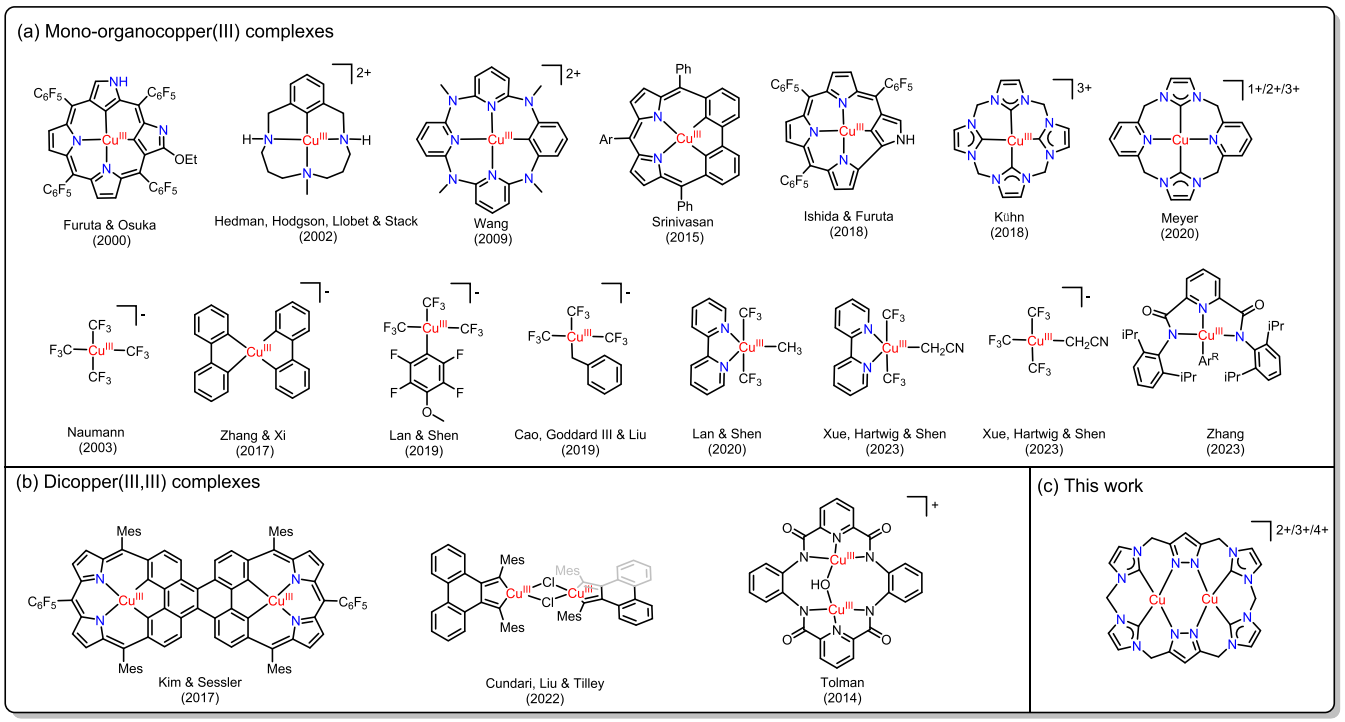

Figure 1. Represented examples of previously reported organocopper(III) complexes and the binuclear copper complexes in the distinct oxidation states (II/II, II/III, and III/III) reported in this work.

Scheme 1. Synthesis of the Complexes 1, 2, and 3

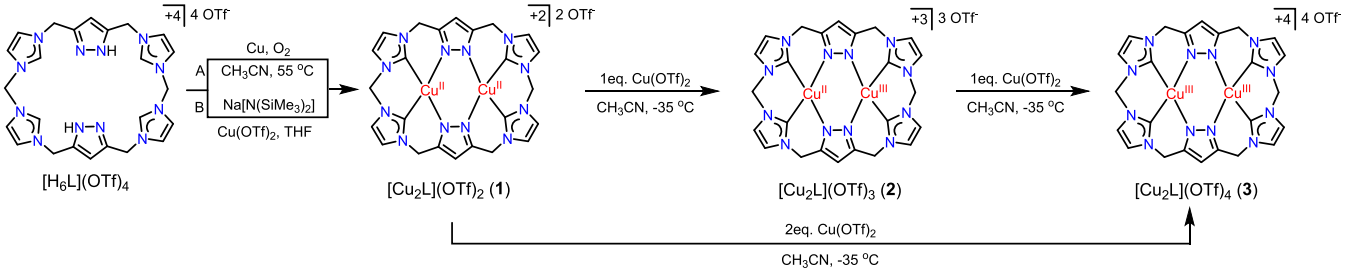

and their redox chemistry is generally associated with decomposition or significant structural changes.[23,53−59] Considering these factors, we propose that the macrocycle polycarbene ligand, featuring two $\{C_2^{NHC}N_2^{pyrazole}\}$ subunits, can trap high-valent diorganocopper complexes in different oxidation states (Figure 1c). This proposal is supported by the successful use of this ligand in synthesizing square-planar coordination bimetallic platinum group complexes $[M_2L](PF_6)_2$ (M = Ni, Pd, Pt),[60−62] demonstrating its potential to stabilize higher valent organocopper complexes.

Herein, we present a diorganocopper system exhibiting three distinct oxidation states—$[Cu^{II}Cu^{II}]$, $[Cu^{II}Cu^{III}]$, and $[Cu^{III}Cu^{III}]$—within a single host scaffold, without significant structural modifications. The structure in question was corroborated by both experimental and theoretical evidence. Notably, the unpaired electron in the mixed-valence complex **2** was found to be localized on a single Cu ion. This complex was thoroughly characterized by using XRD and multiple spectroscopic methods, including NMR, UV−vis−NIR, diffuse reflectance spectroscopy (DRS), and EPR, in addition to DFT calculations. These findings highlight a distinction between the mixed-valence complex **2** and the resting state of the biological Cu_A center,[63] which is a fully delocalized mixed-valent dicopper form.

RESULTS AND DISCUSSION

Synthesis and Redox Properties of Diorganocopper(II,II) Complex

A dicopper(II,II) complex, $[Cu_2L](OTf)_2$ (**1**), can be obtained via reacting $[H_6L](OTf)_4$ with an excess copper powder in CH_3CN under O_2 atmosphere. However, the isolated yield is low (ca. 22%). According to the relevant literature,[58] we assumed that the side products are probably caused by the reaction of $[H_6L](OTf)_4$ with Cu_2O freshly generated from copper oxidation under weakly acidic conditions. Expectedly, the reaction of $[H_6L](OTf)_4$ with an excess Cu_2O in acetonitrile did afford an unusual complex $[Cu_8L_2](OTf)_4$, which decomposed slowly in air (see Supporting Information, Scheme S3). Overall, the intermediate of this reaction may be complex $[Cu_8L_2](OTf)_4$; however, it also afforded other side products, which is still unclear. Besides, the initial deprotonation of $[H_6L](OTf)_4$ with $Na[N(SiMe_3)_2]$ in THF, followed by treatment with $Cu(OTf)_2$ led to the isolation of complex **1** in 17% yield, as illustrated in Scheme 1. The formation of

https://doi.org/10.1021/jacsau.4c00745
JACS Au 2024, 4, 4406−4414

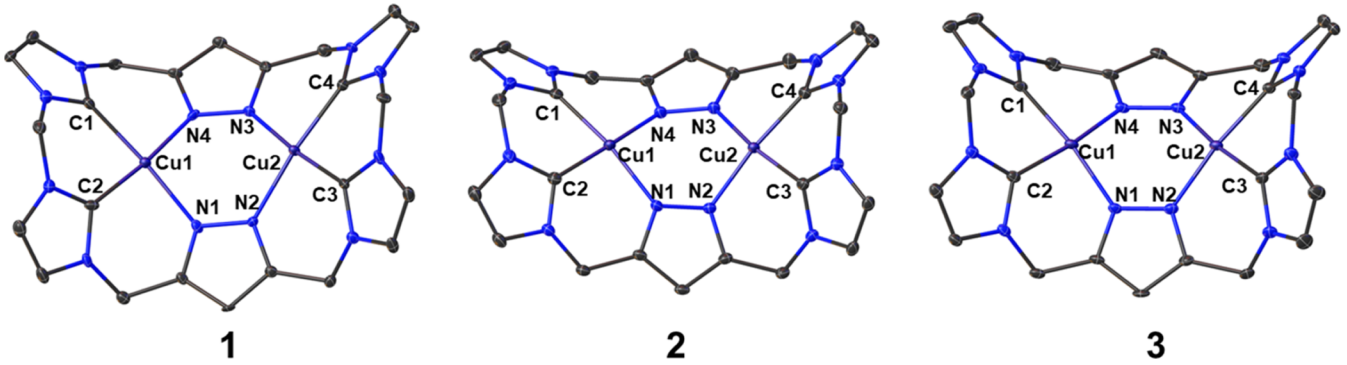

Figure 2. ORTEP plots (50% probability) of the crystal structures of the cations of **1**, **2**, and **3**. Hydrogen atoms, lattice solvent (CH_3CN), and anions are omitted for clarity. Selected atom distances and angles of **1**, **2**, and **3** are listed in Table 1.

Table 1. Selected Distances [Å], Bond Lengths [Å], and Angles [deg] for 1, 2, and 3

complexes	1	2	3	complexes	1	2	3
C1−Cu1 (Å)	1.985(7)	1.962(3)	1.916(7)	C1−Cu1−C2 (deg)	86.10(3)	88.02(13)	84.30(3)
C2−Cu1 (Å)	1.981(7)	1.988(2)	1.888(7)	C1−Cu1−N1 (deg)	175.20(2)	170.04(11)	172.70(3)
N1−Cu1 (Å)	1.998(5)	1.903(3)	1.899(6)	C2−Cu1−N4 (deg)	174.55(2)	174.57(12)	173.00(3)
N4−Cu1 (Å)	1.999(6)	1.970(3)	1.902(6)	N1−Cu1−N4 (deg)	96.10(2)	93.15(10)	96.17(2)
C3−Cu2 (Å)	1.979(6)	1.899(3)	1.890(8)	C3−Cu2−C4 (deg)	87.07(2)	84.25(13)	84.10(3)
C4−Cu2 (Å)	1.982(6)	1.896(3)	1.889(7)	C3−Cu2−N3 (deg)	174.80(2)	171.05(12)	173.40(3)
N2−Cu2 (Å)	2.004(5)	1.894(3)	1.892(6)	C4−Cu2−N2 (deg)	173.90(2)	172.51(12)	172.40(3)
N3−Cu2 (Å)	2.011(5)	1.990(3)	1.883(6)	N2−Cu2−N3 (deg)	96.40(2)	98.16(11)	96.60(2)
Cu1−Cu2 (Å)	3.649	3.657	3.530	dihedral angle (deg)	59.55	131.90	56.25

complex **1** is confirmed by high-resolution electrospray ionization (HR-ESI) mass spectrometry (see Supporting Information, Figure S2) and by single-crystal X-ray diffraction (Figure 2). Complex **1** is stable in both the solid state and in CH_3CN solution under an inert atmosphere (Ar or N_2) at room temperature. X-ray crystallography reveals that complex **1** contains two crystallographically equivalent Cu^{II} centers, each hosted within a $\{C_2^{NHC}N_2^{pyrazole}\}$ subunit of ligand $[H_6L](OTf)_4$. Each Cu^{II} center is coordinated with two pyrazol nitrogen atoms and two NHC donors, resulting in a planar but twisted coordination geometry (τ_4 = 0.07). The $Cu^{II}-C^{NHC}$ bond lengths (approximately 1.98 Å) are slightly longer than those of $Cu^{I}-C^{NHC}$.[55,64] The Cu1···Cu2 distance of 3.649 Å in complex **1** is too great to suggest a significant coprophilic Cu1···Cu2 interaction (Table 1). The $\{C_2^{NHC}Cu1N_2^{pyrazole}\}$ unit is nearly coplanar, forming a dihedral angle of 59.55° with the plane defined by the $\{C_2^{NHC}Cu2N_2^{pyrazole}\}$ (Table 1). These structure features define the overall structure of complex **1**, reminiscent of the conformations exhibited by macrocyclic ligand in the four-coordinate bimetallic platinum group complexes $[M_2L](PF_6)_2$ (M = Ni, Pd, Pt).[60,62] Furthermore, weak antiferromagnetic coupling between the two S = 1/2 Cu(II) centers was confirmed by superconducting quantum interference device (SQUID) magnetometry on a powder sample (1.8−300 K, J = −13.1 cm^{-1}, Figure 3). As a result, the paramagnetism of complex **1** precludes NMR spectroscopic characterizations at ambient temperature (see Supporting Information, Figure S1).

Subsequently, the redox properties of complex **1** were investigated electrochemically using cyclic voltammetry, as depicted in Figure 4a. An electrochemical series comprising two reversible redox steps is discerned, characterized by half-wave potentials ($E_{1/2}$) of 0.02 and 0.25 V (relative to $Fc^{+/0}$, Figure 4a). This reversibility was confirmed by a linear

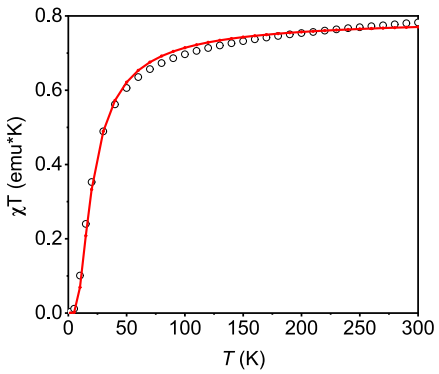

Figure 3. SQUID data for $[Cu(L)_2]^{2+}$ (black circles) recorded in the temperature range 1.8−300 K, at an applied magnetic field of 1 T. Simulations (red solid lines) provide the following parameters: g = 2.06, J = −13.1 cm^{-1}, and temperature-independent paramagnetism TIP = 220 × 10^{-6} emu/mol.

dependence of the current on the square root of the scan rate, consistent with Randles−Sevcik equation (refer to Supporting Information, Figures S14 and S15 for details). Notably, the oxidation potential of complex **1** is comparatively lower than those reported for many Cu^{II} or Cu^{III} complexes with anionic N- or C-donor ligands.[65] The reversible redox behavior of **1** also suggests that the macrocyclic ligand possesses the necessary structural and electronic pliability to accommodate all three oxidation states, ranging from $Cu^{II}Cu^{II}$, through $Cu^{II}Cu^{III}$, to $Cu^{III}Cu^{III}$, within this dicopper framework. In parallel, the comproportionation constant (K_c) for complex **2** was determined to be 7.8 × 10^3, as calculated from the potential separation ($\Delta E_{1/2}$) associated with the sequential oxidation of the two Cu(II) ions, indicative of the thermodynamic stability of the mixed-valent species.[66]

https://doi.org/10.1021/jacsau.4c00745
JACS Au 2024, 4, 4406−4414

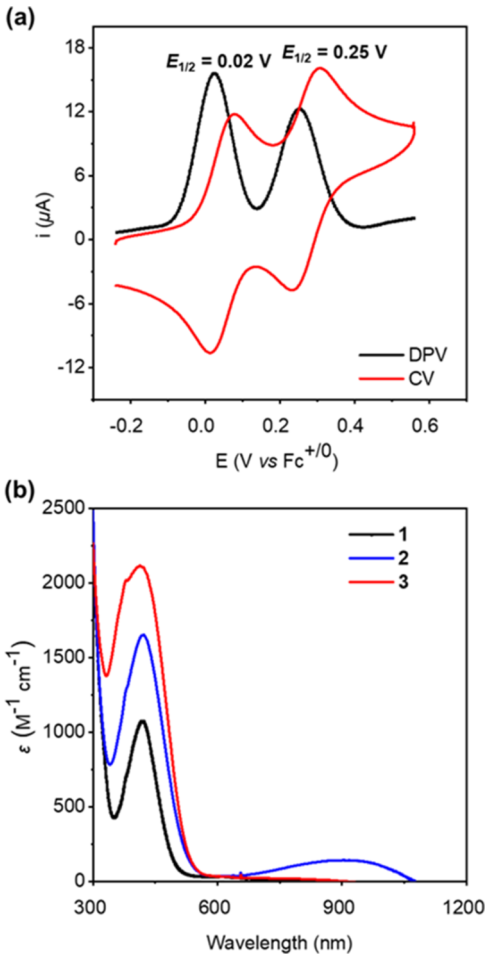

Figure 4. (a) Cyclic voltammogram and DPV of complex $[Cu_2L](OTf)_2$ (**1**) in CH_3CN (0.1 M) $[nBu_4N](PF_6)$ at 298 K, conditions: working electrode: glassy carbon electrode; reference electrode: Ag^+/Ag; scan rate = 100 mV/s. (b) UV−vis spectra of $[Cu_2L](OTf)_2$ (**1**), $[Cu_2L](OTf)_3$ (**2**), and $[Cu_2L](OTf)_4$ (**3**) (0.4 mM) in CH_3CN at 233 K.

To further investigate the specified species ($Cu^{II}Cu^{III}$ and $Cu^{III}Cu^{III}$), chemical oxidation of complex **1** was initially performed at −40 °C and monitored using UV−vis spectroscopy. The UV−vis spectrum of complex **1** exhibits a pronounced band at 420 nm (ε = 1068 M^{-1} cm^{-1}, Figure 4b). The addition of $Cu(OTf)_2$[67] to a solution of complex **1** in acetonitrile led to an increase in the intensity of the band at λ_{max} = 420 nm, as well as the emergence of a broad feature extending into the near-IR (Figure 4b). Titration experiments suggested that these new spectral features reached maximum intensity upon the addition of 1 equiv of $Cu(OTf)_2$ (Figure S12a). Notably, when more than 1 equiv of $Cu(OTf)_2$ was added, the feature of 420 nm became approximately twice as intense as that of complex **1**, while a distinct feature in the NIR region disappeared (Figures 4b and S12b). These results indicate that the absorption at 420 nm and the broad absorption around 1000 nm could be attributed to ligand-to-metal (LMCT) transitions and the metal-to-metal intervalence charge transfer transition, respectively. The oxidized products are stable in CH_3CN solution under Ar atmosphere at −40 °C. However, they slowly decompose in CH_3CN solution at room temperature, as evidenced by UV−vis spectroscopy (Figure S11). These findings suggest that the preparation and isolation of the oxidized diorganocopper complexes through chemical oxidation is viable.

Structural Characterization of Diorganocopper(II,III) Complex

We synthesized the diorganocopper(II,III) complex $[Cu_2L](OTf)_3$ (**2**) using $Cu(OTf)_2$[67] as oxidant. The complex was obtained as an orange solid in high yield (approximately 95% yield) (Schemes 1 and S4). The HR-ESI mass spectrum of complex **2** (in positive-ion mode, Figure S4) exhibited peaks at m/z = 903.9676, m/z = 376.5084, and m/z = 201.3550, corresponding to $[[Cu_2L](OTf)_2]^+$ (calcd 903.9701), $[[Cu_2L](OTf)]^{2+}$ (calcd 376.5095), and $[Cu_2L]^{3+}$ (calcd 201.3555), respectively. Crystals of complex **2** were obtained by slow diffusion of Et_2O into a saturated CH_3CN solution of the crude material at −35 °C (Figure 2). The structure of complex **2** in the solid state closely resembled that of complex **1** (Figure 7), indicating a low reorganization energy for the $1e^-$ oxidation complex **1**. Analysis of the $Cu-C^{NHC}$ bonds revealed that the $Cu-C^{NHC}$ bonds of Cu2 (1.899(3) and 1.896(3) Å) in complex **2** were considerably shorter than the $Cu-C^{NHC}$ bonds of Cu1 (1.962(3) and 1.988(2) Å), but the latter are almost identical to the Cu1 bonds in dicopper(II, II) complex **1** (1.985(7) and 1.981(7) Å), as well as Cu2−C^{NHC} bonds (1.979(6) and 1.982(6) Å). This observation is consistent with the expectation that the increased electron deficiency of the metal center enhances its interaction with the carbene donors.[38] Furthermore, oxidation of **1** to **2** led to significantly shortened $Cu-N^{pyrazole}$ distances (Table 1), indicating that the one-electron oxidation primarily occurred at the Cu2 center.

The X-band EPR spectrum of **2** recorded at 295 K in fluid CH_3CN solution displays a quartet (Figure 5a). This arises from the hyperfine interaction with one Cu nucleus, indicative of the predominant localization of the sole unpaired electron of **2** on a single Cu center. A powder sample of **2** also elicits an analogous EPR spectrum (Figure S21). The g and A anisotropy were resolved in the 120 K spectrum measured for **2** in a frozen ^{n}PrCN/CH_3CN (5:1) solution (Figure 5b). Satisfactory simulations with EasySpin software package[68] yield $g_{||}$ = 2.1174, $g_\perp$ = 2.0291, and $A_{||}(^{63}Cu/^{65}Cu)$ = 639 MHz, $A_\perp$ = 108 MHz. The observed anisotropic patterns of g and A tensors ($g_{||} > g_\perp > 2.0$ and $|A_{||}| > |A_\perp|$) are typical of mononuclear square-planar cupric species distinguished by the d_{x2-y2}-based singly occupied molecular orbital (SOMO).[69] The superhyperfine splitting was found to originate from two equivalent ^{14}N nuclei (I = 1, natural abundance 99.6%) with $A_{iso}(^{14}N)$ = 52 MHz, which suggests delocalization of the spin density onto the diazole N atoms due to the strong covalent interaction between Cu and the diazole ligands. Notably, the slight difference in the nuclear g values of ^{63}Cu and ^{65}Cu isotopes (^{63}Cu I = 3/2, natural abundance 69.2%, g = 1.4824, and ^{65}Cu I = 3/2, natural abundance 30.8%, g = 1.5878) is manifest in the lowest- and highest-field longitudinal hyperfine lines of $^{63}Cu/^{65}Cu$ (Figure 5b, insets).[70] Our repeated attempts to fit the spectrum recorded at 295 K (Figure 5a) showed that at this temperature, the system does not tumble fast enough to be in the fast-motion regime. Consequently, simulations invoking the slow-motion approximation produce a reasonable solution with rotational correlation time $t = 7.5 \times 10^{-11}$ s alongside the fixed g and A values determined above.

To further probe the electronic structures of **1** and **2**, UV−vis−NIR absorption spectra were collected for CH_3CN solutions of **1** and **2** at 298 K (Figure 6). The UV−vis−NIR

https://doi.org/10.1021/jacsau.4c00745
JACS Au 2024, 4, 4406−4414

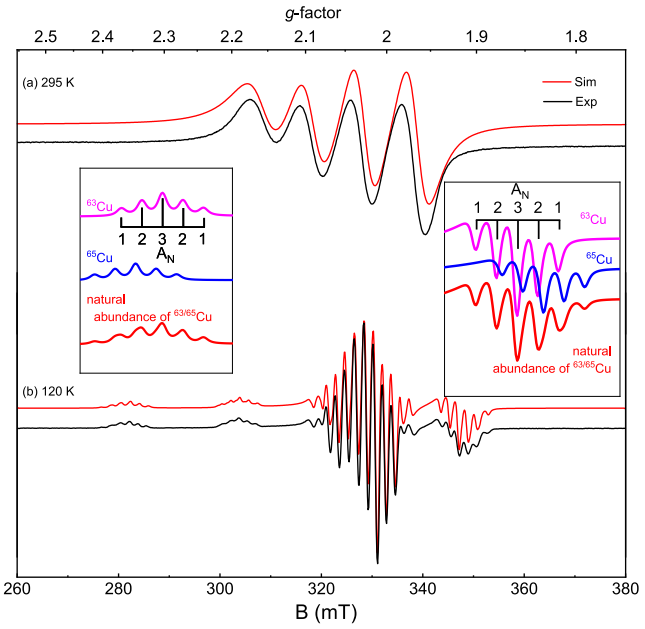

Figure 5. (a) EPR spectrum of **2** (black line) recorded in fluid CH_3CN solution at 295 K. Simulation (red line) with fixed $g_{\|}$ = 2.1174, $g_{\perp}$ = 2.0291, and $A_{\|}(^{63}Cu/^{65}Cu)$ = 639 MHz, $A_{\perp}(^{63}Cu/^{65}Cu)$ = 108 MHz gives rotational correlation time $t = 7.5 \times 10^{-11}$ s. Acquisition conditions: microwave frequency = 9.33431 GHz, power = 1 mW, modulation amplitude = 12 G. (b) EPR spectrum of **2** (black line) recorded in frozen ^{n}PrCN/CH_3CN (5:1) solution at 120 K. Simulation (red line) gives $g_{\|}$ = 2.1174, $g_{\perp}$ = 2.0291, and $A_{\|}(^{63}Cu/^{65}Cu)$ = 639 MHz, $A_{\perp}(^{63}Cu/^{65}Cu)$ = 108 MHz; $A_{iso}(^{14}N)$ = 52 MHz. Acquisition conditions: microwave frequency = 9.329897 GHz, power = 1 mW, modulation amplitude = 5 G. Inset: simulations using 100% ^{63}Cu (purple line), 100% ^{65}Cu (blue line), and natural abundance of $^{63}Cu/^{65}Cu$ (red line) nuclei.

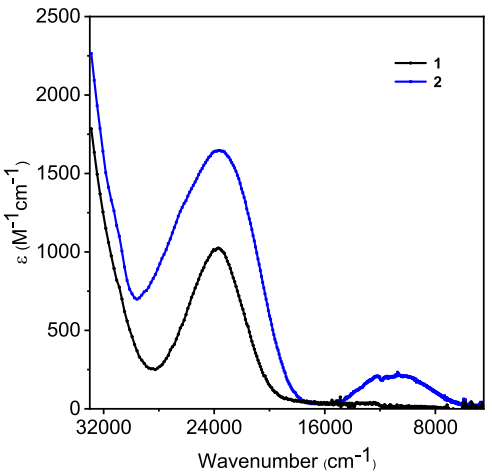

Figure 6. Electronic spectra of complexes **1** (black line) and **2** (blue line) in CH_3CN solution.

spectrum of **1** exhibits an intense band at 23 740 cm^{-1} ($\varepsilon \sim$ 1020 M^{-1} cm^{-1}). TD-DFT calculations indicate that this band is attributed to the d-d transitions at each Cu(II) site and crossing the two Cu(II) sites. Upon one-electron oxidation, this feature is broadened with the maximum shifting to 23 500 cm^{-1}, and its intensity rises ($\varepsilon \sim$ 1620 M^{-1} cm^{-1}). Considering the variation of the intensity, we assign this feature to a ligand-to-metal (LMCT) transition. TD-DFT calculations support this assignment. Importantly, for complex **2**, a new, weak band (ε_{max} = 210 M^{-1} cm^{-1}) emerges in the near-IR region centered at 10600 cm^{-1}, which is attributed to the metal-to-metal intervalence charge transfer transition (IVCT). TD-DFT calculations of **2** in CH_3CN solution also showed an intense band arising from the Cu1-$d_{x_2-y_2}$-based σ^* to Cu2-$d_{x_2-y_2}$-based σ^* orbital at 9370 cm^{-1} (for details, see the Supporting Information), in line with the observed spectrum. The solid-state powder spectrum of **2** measured with diffuse reflectance spectroscopy (DRS, Figure S23) shows absorption bands at 440 and 900 nm, in analogy to that found for the solution sample. The band shape analysis of this Gaussian-shaped absorption based on Hush's theory gives half-height $\Delta\nu_{1/2}{}^0$ = 4460 cm^{-1} that is in reasonable agreement with $\Delta\nu_{1/2}$ = 5250 cm^{-1} observed experimentally, and the effective electronic coupling matrix element H_{ab} = 610 cm^{-1} for weakly interacting centers (for details, see the Supporting Information). Given that $2H_{ab}/\lambda$ = 0.11, complex **2** is best described as being close to the borderline between valence-trapped or charge-localized class I systems and charge moderately delocalized class II systems in Robin and Day classification,[71] consistent with the view inferred from EPR measurements. Furthermore, neither temperature dependence nor solvent dependence was found for the IVCT feature of complex **2** (Figures S24 and S25), corroborating the aforementioned assignment.

Synthesis and Structural Characterization of Diorganocopper(III,III) Complex

Given the above results, we reacted complex **1** with 2 equiv $Cu(OTf)_2$[67] to give diamagnetic $[Cu_2L](OTf)_4$ (**3**) as dark-orange solid in high yield (ca. 76%). The diamagnetism of **3** is reflected by sharp ^1H NMR signals in the normal range (0−8.0 ppm in CD_3CN, Figure S5). Any dynamics of the puckered conformation in solution are slow on the NMR time scale, as was observed for $[Ni_2L](PF_6)_2$.[60] Remarkably, the Cu−C resonance is strongly upfield shifted in the ^{13}C NMR spectrum (144.6 ppm, Figure S6), in line with the electron-deficient nature of the Cu^{III} center.[38] But complex **3** is unstable at room temperature, as confirmed by ^1H NMR measurements (Figure S9). Interestingly, the mixtures of **1** and **3** caused species **2** in CH_3CN solution at −40 °C (Figure S13), which indicated the rapid electron transfer (ET) between **1** and **3**. Luckily, dark-orange crystals of **3** suitable for X-ray diffraction analysis were obtained at −35 °C by slow diffusion of Et_2O into a saturated CH_3CN solution. As shown in Figure 2, the structure of complex **3** in solid state is very similar to that of the **1** and **2** (Figure 7). Further oxidation of **1** led to significantly shortening of the Cu1−C^{NHC} bond lengths from 1.962(3) and 1.988(2) Å in **2** to 1.916(7) and 1.888(7) Å in **3** (Table

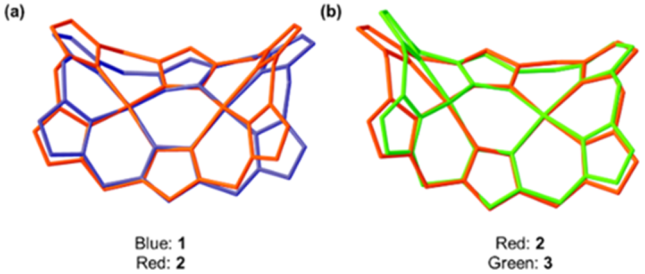

Figure 7. (a) Overlay of the cations of **1** (blue) and **2** (red); (b) overlay of the cations of **3** (green) and **2** (red).

https://doi.org/10.1021/jacsau.4c00745
JACS Au 2024, 4, 4406−4414

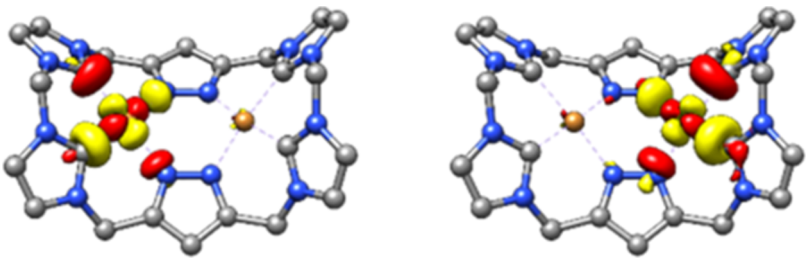

Figure 8. Cu1-$d_{x_2-y_2}$-based singly occupied MO and the corresponding Cu2-$d_{x_2-y_2}$-based unoccupied MO of complex **2** (using the PBE0 functional and def2-TZVP basis set).

1), in agreement with those reported for $Cu^{III}-C^{NHC}$ (1.879–1.884 Å).[37,38]

DFT Calculation and Electron Structure Analysis

To gain more insight into the electronic structures of this series of binuclear copper complexes, detailed DFT calculations were performed. For complex **1**, the open-shell singlet featuring two antiferromagnetically coupled Cu^{II} centers was calculated to be stabilized by more than 35.6 kcal/mol compared to the closed-shell singlet, but close in energy with a marginal difference of 1.2 kcal/mol to the corresponding triplet state having the two ferromagnetically coupled fragments. According to the formula developed by Yamaguchi et al.,[72,73] a coupling constant of $J = -15.2$ cm^{-1} was calculated, which is in excellent agreement with the experimental J value of -13.1 cm^{-1} measured by SQUID magnetometry. As such, DFT computations qualitatively reproduce the experimental findings, in particular the weak antiferromagnetic coupling found for complex **1**.

The computed structure of complex **2** shows that the two Cu ions feature disparate Cu–N and Cu–C distances with a long Cu···Cu separation of 3.51 Å, all in accordance with its X-ray structure (Table S4). Relative to **1**, complex **2** features more covalent Cu-ligand bonding as a consequence of the metal-centered oxidation. The SOMO is the Cu1-$d_{x_2-y_2}$-based σ^* antibonding molecular orbital (MO) with appreciable contributions from N-$p_{x,y}$ and C-$p_{x,y}$ atomic orbitals, while the corresponding MO with a predominant Cu2-$d_{x_2-y_2}$ parentage is unoccupied (Figure 8). In line with this, the computed spin density is largely located on the Cu1 center (51%) and has a negligible contribution from Cu2 (1%) (Figure S33). Thus, their mutual electron transfer from Cu1 to Cu2 is severely hindered by extremely low orbital overlap arising from the unfavorable orientation of the two coordinating planes. These findings rationalize its weak IVCT absorption and the four-line pattern of the Cu hyperfine interaction in its EPR spectra.

CONCLUSIONS

In this study, we synthesized, isolated, and structurally characterized a diorganocopper system in three distinct redox states: $[Cu^{II}Cu^{II}]$, $[Cu^{II}Cu^{III}]$, and $[Cu^{III}Cu^{III}]$. These redox states were supported by a macrocyclic ligand scaffold that features two square-planar coordination $\{C_2^{NHC}N_2^{pyrazole}\}$ compartments. Notably, this work presents the first report on the structural determination of mixed-valence diorganocopper(II,III) complex **2**. Through crystallographic and spectroscopic investigations, it was found that complex **2** is at the borderline between valence-trapped or charge-localized class I systems and charge moderately delocalized class II systems in Robin and Day classification. Additionally, the UV/vis–NIR spectroscopy and TD-DFT calculation provided insights into the electronic structure of the mixed-valence complex **2** in solution. In summary, these findings enhance our understanding of the systematic changes in structure and electronic state in diorganocopper complexes accompanying variations in redox states. This work suggests that such binuclear complexes may serve as a promising bioinspired molecular framework for probing multielectron transformation processes. Ongoing investigations are hence being conducted to explore their applications and further understand their capabilities.

METHODS

Ligand $[H_6L](OTf)_4$ was synthesized according to the procedures described in the literature.[60] Experiments involving air- or moisture-sensitive reagents were performed using standard Schlenk techniques under an argon atmosphere or in a glovebox. Solvents were freshly distilled according to standard procedures prior to use. Glassware was dried in an oven at 90 °C before use. Deionized water was further purified using a Milli-Q ultrapure water purification system. ^1H and $^{13}C\{^1H\}$ NMR spectra were recorded on a 400 MHz Bruker Biospin Advance III NMR spectrometer. ESI-HRMS spectra were measured on LCMS-IT/TOF instruments (Shimadzu and Thermo U3000+). UV–vis measurements were recorded using an Agilent Cary 60 UV–vis spectrometer or an Agilent Cary 8454 UV–vis spectrometer. The C H N elements content was evaluated by EuroVector elemental analyzer. The electrochemical measurements were carried out with the three-electrode system using a CHI-660E electrochemical workstation. Single crystals suitable for X-ray diffraction measurement were collected with a Rigaku Agilent SuperNova Dual system at 173 K. Continuous-wave (cw) X-band EPR measurements were performed on a Bruker A200 spectrometer equipped with a high-sensitivity cavity (ER4119HS) in conjunction with microwave bridge Bruker A40X. Magnetic susceptibility data were measured from powder samples of solid material in the temperature range 1.8–300 K by using a SQUID magnetometer with a field of 1 T. UV–vis–NIR spectra were recorded with a SHIMADZU UV-3600i Plus spectrophotometer.

ASSOCIATED CONTENT

Supporting Information

The Supporting Information is available free of charge at https://pubs.acs.org/doi/10.1021/jacsau.4c00745.

Additional experimental details, materials, methods, complexes synthesis (NMR and ESI-HRMS), X-ray crystallography, EPR, SQUID, UV–vis, electrochemical studies, DFT calculations, and so on (PDF)

Accession Codes

CCDC 2322758, 2322756, and 2322757 contain the supplementary crystallographic data for this paper. These data can be obtained free of charge via www.ccdc.cam.ac.uk/data_request/cif, by emailing data_request@ccdc.cam.ac.uk,

https://doi.org/10.1021/jacsau.4c00745
JACS Au 2024, 4, 4406–4414

or by contacting The Cambridge Crystallographic Data Centre, 12 Union Road, Cambridge CB2 1EZ, UK; fax: + 44 1223 336033.

AUTHOR INFORMATION

Corresponding Authors

Shengfa Ye − *State Key Laboratory of Catalysis, Dalian Institute of Chemical Physics, Chinese Academy of Sciences, Dalian 116023, China;* orcid.org/0000-0001-9747-1412; Email: shengfa.ye@dicp.ac.cn

Ming-Tian Zhang − *Center of Basic Molecular Science (CBMS), Department of Chemistry, Tsinghua University, Beijing 100084, China;* orcid.org/0000-0001-8808-9641; Email: mtzhang@mail.tsinghua.edu.cn

Authors

Kai Hua − *Center of Basic Molecular Science (CBMS), Department of Chemistry, Tsinghua University, Beijing 100084, China*

Fei Xie − *State Key Laboratory of Catalysis, Dalian Institute of Chemical Physics, Chinese Academy of Sciences, Dalian 116023, China*

Complete contact information is available at: https://pubs.acs.org/10.1021/jacsau.4c00745

Author Contributions

§K.H. and F.X. contributed to the work equally and should be regarded as cofirst authors.

Notes

The authors declare no competing financial interest.

ACKNOWLEDGMENTS

We acknowledge the National Natural Science Foundation of China (NSFC 21933007, 22193011, and 92161204) and Dalian Institute of Chemical Physics, Chinese Academy of Sciences (DICP I202312) for funding support.

REFERENCES

(1) Allen, S. E.; Walvoord, R. R.; Padilla-Salinas, R.; Kozlowski, M. C. Aerobic Copper-Catalyzed Organic Reactions. *Chem. Rev.* **2013**, *113*, 6234−6458.

(2) Zhang, Q.; Tong, S.; Wang, M. X. Unraveling the Chemistry of High Valent Arylcopper Compounds and Their Roles in Copper-Catalyzed Arene C-H Bond Transformations Using Synthetic Macrocycles. *Acc. Chem. Res.* **2022**, *55*, 2796−2810.

(3) Casitas, A.; Ribas, X. The Role of Organometallic Copper(III) Complexes in Homogeneous Catalysis. *Chem. Sci.* **2013**, *4*, 2301−2318.

(4) Hickman, A. J.; Sanford, M. S. High-Valent Organometallic Copper and Palladium in Catalysis. *Nature* **2012**, *484*, 177−185.

(5) Luo, Y. R.; Li, Y. L.; Wu, J.; Xue, X. S.; Hartwig, J. F.; Shen, Q. L. Oxidative Addition of An Alkyl Halide to Form a Stable Cu(III) Product. *Science* **2023**, *381*, 1072−1079.

(6) Liu, L.; Xi, Z. F. Organocopper(III) Compounds with Well-Defined Structures Undergo Reductive Elimination to Form C-C or C-Heteroatom Bonds. *Chin. J. Chem.* **2018**, *36*, 1213−1221.

(7) Tang, X. D.; Wu, W. Q.; Zeng, W.; Jiang, H. Copper-Catalyzed Oxidative Carbon−Carbon and/or Carbon-Heteroatom Bond Formation with O_2 or Internal Oxidants. *Acc. Chemi. Res.* **2018**, *51*, 1092−1105.

(8) Elwell, C. E.; Gagnon, N. L.; Neisen, B. D.; Dhar, D.; Spaeth, A. D.; Yee, G. M.; Tolman, W. B. Copper-Oxygen Complexes Revisited: Structures, Spectroscopy, and Reactivity. *Chem. Rev.* **2017**, *117*, 2059−2107.

(9) Zhang, H.-T.; Xie, F.; Guo, Y. H.; Xiao, Y.; Zhang, M. T. Selective Four-Electron Reduction of Oxygen by a Nonheme Heterobimetallic CuFe Complex. *Angew. Chem., Int. Ed.* **2023**, *62*, No. e202310775.

(10) Chen, Q. F.; Cheng, Z. Y.; Liao, R. Z.; Zhang, M. T. Bioinspired Trinuclear Copper Catalyst for Water Oxidation with a Turnover Frequency up to 20000 s^{-1}. *J. Am. Chem. Soc.* **2021**, *143*, 19761−19768.

(11) Halvagar, M. R.; Solntsev, P. V.; Lim, H.; Hedman, B.; Hodgson, K. O.; Solomon, E. I.; Cramer, C. J.; Tolman, W. B. Hydroxo-Bridged Dicopper(II,III) and -(III,III) Complexes: Models for Putative Intermediates in Oxidation catalysis. *J. Am. Chem. Soc.* **2014**, *136*, 7269−7272.

(12) Liu, Y.; Chatterjee, S.; Cutsail, G. E., III; Peredkov, S.; Gupta, S. K.; Dechert, S.; DeBeer, S.; Meyer, F. Cu_4S Cluster in ″0-Hole″ and ″1-Hole″ States: Geometric and Electronic Structure Variations for the Active Cu_Z* Site of N_2O Reductase. *J. Am. Chem. Soc.* **2023**, *145*, 18477−18486.

(13) Gennari, M.; Pecaut, J.; DeBeer, S.; Neese, F.; Collomb, M. N.; Duboc, C. A Fully Delocalized Mixed-Valence Bis-μ(thiolato) Dicopper Complex: a Structural and Functional Model of the Biological Cu_A Center. *Angew. Chem., Int. Ed.* **2011**, *50*, 5662−5666.

(14) Su, X. J.; Gao, M.; Jiao, L.; Liao, R. Z.; Siegbahn, P. E. M.; Cheng, J. P.; Zhang, M. T. Electrocatalytic Water Oxidation by a Dinuclear Copper Complex in a Neutral Aqueous Solution. *Angew. Chem., Int. Ed.* **2015**, *54*, 4909−4914.

(15) Torelli, S.; Orio, M.; Pecaut, J.; Jamet, H.; Le Pape, L.; Menage, S. A $\{Cu_2S_2\}^+$ Mixed-Valent Core Featuring a Cu-Cu Bond**. *Angew. Chem., Int. Ed.* **2010**, *49*, 8249−8252.

(16) Isaac, J. A.; Gennarini, F.; Lopez, I.; Thibon-Pourret, A.; David, R.; Gellon, G.; Gennaro, B.; Philouze, C.; Meyer, F.; Demeshko, S.; Le Mest, Y.; Reglier, M.; Jamet, H.; Le Poul, N.; Belle, C. Room-Temperature Characterization of a Mixed-Valent μ-Hydroxodicopper-(II,III) Complex. *Inorg. Chem.* **2016**, *55*, 8263−8266.

(17) Bergman, H. M.; Beattie, D. D.; Handford, R. C.; Rossomme, E.; Suslick, B. A.; Head-Gordon, M.; Cundari, T. R.; Liu, Y.; Tilley, T. D. Copper(III) Metallacyclopentadienes via Zirconocene Transfer and Reductive Elimination to an Isolable Phenanthrocyclobutadiene. *J. Am. Chem. Soc.* **2022**, *144*, 9853−9858.

(18) Keown, W.; Gary, J. B.; Stack, T. D. P. High-Valent Copper in Biomimetic and Biological Oxidations. *JBIC, J. Biol. Inorg. Chem.* **2017**, *22*, 289−305.

(19) Mirica, L. M.; Ottenwaelder, X.; Stack, T. D. P. Structure and Spectroscopy of Copper−Dioxygen Complexes. *Chem. Rev.* **2004**, *104*, 1013−1046.

(20) Solomon, E. I.; Sundaram, U. M.; Machonkin, T. E. Multicopper Oxidases and Oxygenases. *Chem. Rev.* **1996**, *96*, 2563−2606.

(21) Nakamura, E.; Mori, S. Wherefore Art Thou Copper? Structures and Reaction Mechanisms of Organocuprate Clusters in Organic Chemistry. *Angew. Chem., Int. Ed.* **2000**, *39*, 3750−3771.

(22) Ribas, X.; Jackson, D. A.; Donnadieu, B.; Mahia, J.; Parella, T.; Xifra, R.; Hedman, B.; Hodgson, K. O.; Llobet, A.; Stack, T. D. P. Aryl C-H Activation by Cu^{II} to Form an Organometallic Aryl-Cu^{III} Species: A Novel Twist on Copper Disproportionation. *Angew. Chem., Int. Ed.* **2002**, *41*, 2991−2994.

(23) Younesi, Y.; Nasiri, B.; BabaAhmadi, R.; Willans, C.; Fairlamb, I. J. S.; Ariafard, A. Theoretical Rationalisation for The Mechanism of N-heterocyclic Carbene-Halide Reductive Elimination at Cu^{III}, Ag^{III} and Au^{III}. *Chem. Commun.* **2016**, *52*, 5057−5060.

(24) Yao, B.; Wang, D. X.; Huang, Z. T.; Wang, M. X. Room-Temperature Aerobic Formation of a Stable Aryl-Cu(III) Complex and Its Reactions with Nucleophiles:Highly Efficient and Diverse Arene C-H Functionalizations of Azacalix[1]arene[3]pyridine. *Chem. Commun.* **2009**, 2899−2901.

(25) Bower, J. K.; Cypcar, A. D.; Henriquez, B.; Stieber, S. C. E.; Zhang, S. C(sp^3)-H Fluorination with a Copper(II)/(III) Redox Couple. *J. Am. Chem. Soc.* **2020**, *142*, 8514−8521.

(26) DiMucci, I. M.; Lukens, J. T.; Chatterjee, S.; Carsch, K. M.; Titus, C. J.; Lee, S. J.; Nordlund, D.; Betley, T. A.; MacMillan, S. N.; Lancaster, K. M. The Myth of d^8Copper(III). *J. Am. Chem. Soc.* **2019**, *141*, 18508−18520.
(27) Liu, H.; Wu, J.; Jin, Y. X.; Leng, X. B.; Shen, Q. L. Mechanistic Insight into Copper-Mediated Trifluoromethylation of Aryl Halides: The Role of CuI. *J. Am. Chem. Soc.* **2021**, *143*, 14367−14378.
(28) Liu, L.; Zhu, M.; Yu, H. T.; Zhang, W. X.; Xi, Z. Organocopper(III) Spiro Complexes: Synthesis, Structural Characterization, and Redox Transformation. *J. Am. Chem. Soc.* **2017**, *139*, 13688−13691.
(29) Reese, M. S.; Bonanno, M. G.; Bower, J. K.; Moore, C. E.; Zhang, S. Y. C−N Bond Formation at Discrete CuIII−Aryl Complexes. *J. Am. Chem. Soc.* **2023**, *145*, 26810−26816.
(30) Walroth, R. C.; Lukens, J. T.; MacMillan, S. N.; Finkelstein, K. D.; Lancaster, K. M. Spectroscopic Evidence for a $3d^{10}$ Ground State Electronic Configuration and Ligand Field Inversion in $[Cu(CF_3)_4]^{1-}$. *J. Am. Chem. Soc.* **2016**, *138*, 1922−1931.
(31) Yan, W. H.; Carter, S.; Hsieh, C. T.; Krause, J. A.; Cheng, M. J.; Zhang, S. Y.; Liu, W. Copper−Carbon Homolysis Competes with Reductive Elimination in Well-Defined Copper(III) Complexes. *J. Am. Chem. Soc.* **2023**, *145*, 26152−26159.
(32) Zhang, Q.; Liu, Y.; Wang, T.; Zhang, X. H.; Long, C.; Wu, Y. D.; Wang, M. X. Mechanistic Study on Cu(II)-Catalyzed Oxidative Cross-Coupling Reaction between Arenes and Boronic Acids under Aerobic Conditions. *J. Am. Chem. Soc.* **2018**, *140*, 5579−5587.
(33) Grzegorzek, N.; Pawlicki, M.; Szterenberg, L.; Latos-Grazynski, L. Organocopper(II) Complex of 21-Diphenylphosphoryl-Carbaporpholactone Hybrid: A Side-On Coordination Mode of Copper(II). *J. Am. Chem. Soc.* **2009**, *131*, 7224−7225.
(34) Furuta, H.; Maeda, H.; Osuka, A. Doubly N-Confused Porphyrin: A New Complexing Agent Capable of Stabilizing Higher Oxidation States. *J. Am. Chem. Soc.* **2000**, *122*, 803−807.
(35) Adinarayana, B.; Thomas, A. P.; Suresh, C. H.; Srinivasan, A. A 6,11,16-Triarylbiphenylcorrole with an adj-CCNN Core: Stabilization of an Organocopper(III) Complex**. *Angew. Chem., Int. Ed.* **2015**, *54*, 10478−10482.
(36) Maurya, Y. K.; Noda, K.; Yamasumi, K.; Mori, S.; Uchiyama, T.; Kamitani, K.; Hirai, T.; Ninomiya, K.; Nishibori, M.; Hori, Y.; Shiota, Y.; Yoshizawa, K.; Ishida, M.; Furuta, H. Ground-State Copper(III) Stabilized by N-Confused/N-Linked Corroles: Synthesis, Characterization, and Redox Reactivity. *J. Am. Chem. Soc.* **2018**, *140*, 6883−6892.
(37) Liu, Y.; Resch, S. G.; Klawitter, I.; Cutsail, G. E., III; Demeshko, S.; Dechert, S.; Kuhn, F. E.; DeBeer, S.; Meyer, F. An Adaptable N-Heterocyclic Carbene Macrocycle Hosting Copper in Three Oxidation States. *Angew. Chem., Int. Ed.* **2020**, *59*, 5696−5705.
(38) Ghavami, Z. S.; Anneser, M. R.; Kaiser, F.; Altmann, P. J.; Hofmann, B. J.; Schlagintweit, J. F.; Grivani, G.; Kühn, F. E. A Bench Stable Formal Cu(III) N-heterocyclic Carbene Accessible from Simple Copper(II) Acetate. *Chem. Sci.* **2018**, *9*, 8307−8314.
(39) Wang, G. Y.; Li, H. Y.; Leng, X. B.; Lu, L.; Shen, Q. L. Access to Versatile Functionalized Cu(III) Complexes Enabled by Direct Transmetalation to Well-Defined Copper(III) Fluoride Complex $Me_4N^+[Cu(CF_3)_3F]^-$. *Chin. J. Chem.* **2024**, *42*, 1107−1113.
(40) Wang, G. Y.; Li, M.; Leng, X. B.; Xue, X. S.; Shen, Q. L. Neutral Five-Coordinate Arylated Copper(III) Complex: Key Intermediate in Copper-Mediated Arene Trifluoromethylation. *Chin. J. Chem.* **2022**, *40*, 1924−1930.
(41) Liu, S. S.; Liu, H.; Liu, S. H.; Lu, Z. H.; Lu, C. H.; Leng, X. B.; Lan, Y.; Shen, Q. L. $C(sp^3)$-CF_3 Reductive Elimination from a Five-Coordinate Neutral Copper(III) Complex. *J. Am. Chem. Soc.* **2020**, *142*, 9785−9791.
(42) Paeth, M.; Tyndall, S. B.; Chen, L. Y.; Hong, J. C.; Carson, W. P.; Liu, X. W.; Sun, X. D.; Liu, J. J.; Yang, K.; Hale, E. M.; Tierney, D. L.; Liu, B.; Cao, Z.; Cheng, M. J.; Goddard, W. A., III; Liu, W. Csp^3−Csp^3 Bond-Forming Reductive Elimination from Well-Defined Copper(III) Complexes. *J. Am. Chem. Soc.* **2019**, *141*, 3153−3159.
(43) Lu, Z. H.; Liu, H.; Liu, S. H.; Leng, X. B.; Lan, Y.; Shen, Q. L. A Key Intermediate in Copper-Mediated Arene Trifluoromethylation, $[nBu_4N][Cu(Ar)(CF_3)_3]$: Synthesis, Characterization, and $C(sp^2)$−CF_3 Reductive Elimination. *Angew. Chem., Int. Ed.* **2019**, *131*, 8598−8602.
(44) Casitas, A.; King, A. E.; Parella, T.; Costas, M.; Stahl, S. S.; Ribas, X. Direct Observation of Cu^I/Cu^{III} Redox Steps Relevant to Ullmann-type Coupling Reactions. *Chem. Sci.* **2010**, *1*, 326−330.
(45) Naumann, D.; Roy, T.; Tebbe, K. F.; Crump, W. Synthesis and Structure of Surprisingly Stable Tetrakis(trifluoromethyl)cuprate(III) Salts**. *Angew. Chem., Int. Ed.* **1993**, *32*, 1482−1483.
(46) Ke, X. S.; Hong, Y.; Tu, P.; He, Q.; Lynch, V. M.; Kim, D.; Sessler, J. L. Hetero Cu(III)-Pd(II) Complex of a Dibenzo[g,p]-chrysene-Fused Bis-dicarbacorrole with Stable Organic Radical Character. *J. Am. Chem. Soc.* **2017**, *139*, 15232−15238.
(47) Cheng, J.; Wang, L. J.; Wang, P.; Deng, L. High-Oxidation-State 3d Metal (Ti-Cu) Complexes with N-Heterocyclic Carbene Ligation. *Chem. Rev.* **2018**, *118*, 9930−9987.
(48) Peris, E. Smart N-Heterocyclic Carbene Ligands in Catalysis. *Chem. Rev.* **2018**, *118*, 9988−10031.
(49) Charra, V.; de Frémont, P.; Braunstein, P. Multidentate N-heterocyclic Carbene Complexes of the 3d Metals: Synthesis, Structure,Reactivity and Catalysis. *Coord. Chem. Rev.* **2017**, *341*, 53−176.
(50) Hopkinson, M. N.; Richter, C.; Schedler, M.; Glorius, F. An Overview of N-heterocyclic Carbenes. *Nature* **2014**, *510*, 485−496.
(51) Hahn, F. E.; Jahnke, M. C. Heterocyclic Carbenes: Synthesis and Coordination Chemistry. *Angew. Chem., Int. Ed.* **2008**, *47*, 3122−3172.
(52) Liu, Y.; Resch, S. G.; Chen, H.; Dechert, S.; Demeshko, S.; Bill, E.; Ye, S.; Meyer, F. Fully Delocalized Mixed-Valent $Cu^{1.5}$ $Cu^{1.5}$ Complex: Strong Cu-Cu interaction and Fast Electron Self-Exchange Rate Despite Large Structural Changes. *Angew. Chem., Int. Ed.* **2023**, *62*, No. e202215840.
(53) O'Hearn, D. J.; Singer, R. D. Direct Synthesis of a Copper(II) N-Heterocyclic Carbene Complex in Air. *Organometallics* **2017**, *36*, 3175−3177.
(54) Legault, C. Y.; Kendall, C.; Charette, A. B. Structure and Reactivity of a New Anionic N-heterocyclic Carbene Silver(I) Complex. *Chem. Commun.* **2005**, 3826−3828.
(55) Arnold, P. L.; Rodden, M.; Davis, K. M.; Scarisbrick, A. C.; Blake, A. J.; Wilson, C. Asymmetric Lithium(I) and Copper(II) Alkoxy-N-heterocyclic Carbene Complexes; Crystallographic Characterisation and Lewis Acid Catalysis. *Chem. Commun.* **2004**, 1612−1613.
(56) Hu, X. L.; Castro-Rodriguez, I.; Meyer, K. Copper Complexes of Nitrogen-Anchored Tripodal N-Heterocyclic Carbene Ligands. *J. Am. Chem. Soc.* **2003**, *125*, 12237−12245.
(57) Liu, B.; Ma, X. J.; Wu, F. F.; Chen, W. Z. Simple Synthesis of Neutral and Cationic Cu-NHC Complexes. *Dalton Trans.* **2015**, *44*, 1836−1844.
(58) Liu, B.; Liu, B.; Zhou, Y. B.; Chen, W. Z. Copper(II) Hydroxide Complexes of N-Heterocyclic Carbenes and Catalytic Oxidative Amination of Arylboronic Acids. *Organometallics* **2010**, *29*, 1457−1464.
(59) Aaron Lin, S. C.; Liu, Y. H.; Peng, S. M.; Liu, S.-T. Copper(II) Complexes of a Heterotopic N-heterocyclic Carbene Ligand: Preparation and Catalytic Application. *J. Organomet. Chem.* **2018**, *859*, 52−57.
(60) Altmann, P. J.; Jandl, C.; Pöthig, A. Introducing a Pyrazole/Imidazole Based Hybrid Cyclophane: a Hydrogen Bond Sensor and Binucleating Ligand Precursor. *Dalton Trans.* **2015**, *44*, 11278−11281.
(61) Altmann, P. J.; Pöthig, A. Capsoplexes: Encapsulating Complexes via Guest Recognition. *Chem. Commun.* **2016**, *52*, 9089−9092.
(62) Pickl, T.; Pöthig, A. Bimetallic Platinum Group Complexes of a Macrocyclic Pyrazolate/NHC Hybrid Ligand. *Organometallics* **2021**, *40*, 3056−3065.

https://doi.org/10.1021/jacsau.4c00745
JACS Au 2024, 4, 4406−4414

(63) Savelieff, M. G.; Lu, Y. Cu_A Centers and Their Biosynthetic Models in azurin. *J. Biol. Inorg. Chem.* **2010**, *15* (4), 461−483.
(64) Lu, T.; Wang, J. Y.; Tu, D.; Chen, Z. N.; Chen, X. T.; Xue, Z. L. Luminescent Mechanochromic Dinuclear Cu(I) Complexes with Macrocyclic Diamine-Tetracarbene Ligands. *Inorg. Chem.* **2018**, *57*, 13618−13630.
(65) Blusch, L. K.; Craigo, K. E.; Martin-Diaconescu, V.; McQuarters, A. B.; Bill, E.; Dechert, S.; DeBeer, S.; Lehnert, N.; Meyer, F. Hidden Non-Innocence in an Expanded Porphyrin: Electronic Structure of the Siamese-Twin Porphyrin's Dicopper Complex in Different Oxidation States. *J. Am. Chem. Soc.* **2013**, *135*, 13892−13899.
(66) Richardson, D. E.; Taube, H. Mixed-Valence Molecules: Electronic Delocalization and Stabilization. *Coord. Chem. Rev.* **1984**, *60*, 107−129.
(67) Zhang, H.; Yao, B.; Zhao, L.; Wang, D. X.; Xu, B. Q.; Wang, M. X. Direct Synthesis of High-valent Aryl-Cu(II) an Aryl-Cu(III) Compounds: Mechanistic Insight into Arene C-H Bond Metalation. *J. Am. Chem. Soc.* **2014**, *136*, 6326−6332.
(68) Stoll, S.; Schweiger, A. EasySpin, a Comprehensive Software Package for Spectral Simulation and Analysis in EPR. *J. Magn. Reson.* **2006**, *178*, 42−55.
(69) Hathaway, B. J.; Billing, D. E. The Electronic Properties and Stereochemistry of Mono-Nuclear Complexes of the Copper(II) ion. *Coord. Chem. Rev.* **1970**, *5*, 143−207.
(70) Ye, S. F. Probing Electronic Structures of Transition Metal Complexes Using Electron Paramagnetic Resonance Spectroscopy. *Magn. Reson. Lett.* **2023**, *3*, 43−60.
(71) Demadis, K. D.; Hartshorn, C. M.; Meyer, T. J. The Localized-to-Delocalized Transition in Mixed-Valence Chemistry. *Chem. Rev.* **2001**, *101*, 2655−2686.
(72) Yamaguchi, K.; Takahara, Y.; Fueno, T. *Applied Quantum Chemistry*; Smith, V. H., Ed.; Reidel: Dordrecht, 1986; p 155.
(73) Soda, T.; Kitagawa, Y.; Onishi, T.; Takano, Y.; Shigeta, Y.; Nagao, H.; Yoshioka, Y.; Yamaguchi, K. Ab Initio Computations of Effective Exchange Integrals for H−H, H−He−H and Mn_2O_2 Complex: Comparison of Broken-Symmetry Approaches. *Chem. Phys. Lett.* **2000**, *319*, 223−230.

https://doi.org/10.1021/jacsau.4c00745
JACS Au 2024, 4, 4406−4414